photocarriers are generated in the top and bottom cells. However, when the photocurrent-matched configuration is placed in an aqueous environment, the system either produces no current in the external circuit or decomposes (*27*). A thicker, top *p*-type layer and the resultant mismatch of electron-hole formation in the two-junction region appear to be the key for proper operation.

REFERENCES AND NOTES

1. A. J. Bard and M. A. Fox, *Acc. Chem. Res.* **28**, 141 (1995).
2. H. Gerischer, in *Topics in Applied Physics*, vol. 31, Solar Energy Conversion, B. O. Seraphin, Ed. (Springer-Verlag, Berlin, 1979), pp. 115–172.
3. The ability of a semiconductor electrode to drive the electrochemical reaction of interest is determined by its band gap (the energy separation between the valence and conduction band edges) and the position of the valence and conduction band edges relative to the vacuum level (or other reference electrode). In contrast to metal electrodes, semiconductor electrodes in contact with liquid electrolytes have fixed energies where the charge carriers enter the solution. This fixed energy is given by the energetic position of the semiconductor's valence and conduction bands at the surface (where these bands terminate at the semiconductor/electrolyte interface). The energetic position of these band edges is determined by the chemistry of the semiconductor/electrolyte interface, which is controlled by the composition of the semiconductor, the nature of the surface, and the electrolyte composition. So even though a semiconductor electrode may generate sufficient energy to effect an electrochemical reaction, the energetic position of the band edges may prevent it from doing so. For spontaneous water splitting, the oxygen and hydrogen reactions must lie between the valence and conduction band edges, and this is almost never the case.
4. G. E. Shakhnazaryan *et al.*, *Russ. J. Electrochem.* **30**, 610 (1994).
5. E. Aharon-Shalom and A. Heller, *J. Electrochem. Soc.* **129**, 2865 (1982).
6. A. Heller, *Science* **223**, 1141 (1984).
7. S. Kocha, J. Turner, A. J. Nozik, *J. Electroanal. Chem.* **367**, 27 (1991).
8. S. Kocha and J. A. Turner, *J. Electrochem. Soc.* **142**, 2625 (1995).
9. H. Yoneyama, H. Sakamoto, H. Tumura, *Electrochem. Acta* **20**, 341 (1975).
10. A. J. Nozik, *Appl. Phys. Lett.* **29**, 150 (1976).
11. R. C. Kainthla, B. Zelenay, J. O'M. Bockris, *J. Electrochem. Soc.* **134**, 841 (1987).
12. Y. Sakai *et al.*, *Can. J. Chem.* **66**, 1853 (1988).
13. G. Lin *et al.*, *Appl. Phys. Lett.* **55**, 386 (1989).
14. J. Augustynski, G. Calzaferri, J. Courvoisier, M. Graetzel, in *Proceedings of the 11th World Hydrogen Energy Conference*, T. N. Veziroglu, C.-J. Winter, J. P. Baselt, G. Kreysa, Eds. (DECHEMA, Frankfurt, Germany, 1996), pp. 2378–2387.
15. K. A. Bertness *et al.*, *App. Phys. Lett.* **65**, 989 (1994).
16. J. R. Bolton *et al.*, *Nature* **316**, 495 (1985).
17. S. R. Kurtz *et al.*, *J. Appl. Phys.* **68**, 1890 (1990).
18. K. A. Bertness *et al.*, in *AIP Conference Proceedings No. 306*, R. Noufi and H. Ullal, Eds. (American Institute of Physics, New York, 1994), p. 100.
19. O. Khaselev and J. A. Turner, in preparation.
20. For electrochemical measurements, the wafers were cleaved into samples ~0.2 cm^2 in area. The samples with gold ohmic contacts were mounted on a Teflon-covered screw electrode with silver epoxy and heated to 80°C for 1 hour. The electrical contact was insulated from the electrolyte by an epoxy coating that also covered the samples' edges. A conventional two-electrode configuration was used with a platinum gauze or foil counter-electrode coated with ruthenium metal. Photoelectrochemical characteristics were measured with an EG&G 263A potentiostat. The electrolyte, 3 M H_2SO_4, was freshly prepared from deionized water having resistivity of 18 megohm/cm. All solutions were made of analytical-grade reagents. Before electrochemical measurements, the samples were etched in 1:20:1 HCl:CH_3COOH:H_2O_2 solution. A single-compartment cell was used. Although the electrodes were spatially separated, no attempt was made to separate the products of the anode and cathode reactions.
21. To reduce the overvoltage losses associated with the noncatalytic surface of the semiconductor, a thin layer of platinum catalyst was electrochemically deposited on the surface of the semiconductor electrodes from a 20 mM H_2PtCl_6 solution. Photoassisted galvanostatic deposition was performed at a cathodic current density of 1 mA/cm^2, with a platinum quantity corresponding to a charge of 10 mC/cm^2. A recent publication (*28*) has shown that the platinum not only acts as a catalyst for hydrogen evolution but also drastically reduces the corrosion reaction of a similar III-V compound, indium phosphide. We would expect that platinum would offer a comparable corrosion-inhibiting mechanism here.
22. We used concentrated light for two reasons: (i) The photocurrent and the amount of gases produced are higher and therefore easier to quantify, and (ii) because of their cost, the major terrestrial application of the solid-state analog of these tandem cells is in concentrator systems (>100 suns). Therefore, any real application using the present solid-state design for photoelectrolysis would also use concentrated light. However, the PEC systems will probably be limited to less than 100 suns, because that would give rise to a current of about 1A/cm^2, a practical limit for electrolysis. The evolution of gas bubbles on the illuminated surface is also an issue, as these bubbles will scatter light, reducing the efficiency. Given this limitation as well as problems regarding the amount of catalyst and system design issues, a more realistic limit as to the amount of light concentration that can be used for photoelectrolysis is in the range of 10 to 20 suns.
23. The gas products of the photoelectrolysis were analyzed with a UTI-100C mass spectrometer. A sealed cell was used, connected directly to the high-vacuum chamber of the mass spectrometer via a gas inlet system. Before being sealed, the cell was purged for several minutes with nitrogen to remove any oxygen. The cell was then sealed, and the photoelectrolysis reaction was run for several hours. The external current was monitored with an ammeter. Periodically, the gas mixture from the upper part of the cell was sampled by the mass spectrometer system. The same cell was used and the same experimental technique was repeated with the use of two platinum electrodes at the same external current. Within experimental error (~±20%), the results were the same, indicating stoichiometric water splitting.
24. For 100% electrolysis efficiency, this calculation is identical to Bolton's calculation of efficiency (*29*). For the size of these samples and the amount of hydrogen and oxygen being generated, a calculation using external current flow is far more accurate.
25. M. F. Weber and M. J. Dignam, *Int. J. Hydrogen Energy* **11**, 225 (1986).
26. ———, *J. Electrochem. Soc.* **131**, 1258 (1984).
27. S. Kocha, D. Montgomery, M. Peterson, J. A. Turner, *Sol. Energy Mater. Sol. Cells*, in press.
28. P. Bogdanoff, P. Friebe, N. Alonso-Vante, *J. Electrochem. Soc.* **145**, 576 (1998).
29. J. R. Bolton, *Solar Energy* **57**, 37 (1996).

30. We thank S. Kurtz and J. Olson for the tandem cell samples and A. Dillon for help with the mass spectrometer measurements. This work was supported by the Hydrogen Program of the U.S. Department of Energy.

18 November 1997; accepted 23 February 1998

Gastrointestinal Tract as a Major Site of CD4$^+$ T Cell Depletion and Viral Replication in SIV Infection

Ronald S. Veazey, MaryAnn DeMaria, Laura V. Chalifoux, Daniel E. Shvetz, Douglas R. Pauley, Heather L. Knight, Michael Rosenzweig, R. Paul Johnson, Ronald C. Desrosiers, Andrew A. Lackner*

Human and simian immunodeficiency virus (HIV and SIV) replicate optimally in activated memory CD4$^+$ T cells, a cell type that is abundant in the intestine. SIV infection of rhesus monkeys resulted in profound and selective depletion of CD4$^+$ T cells in the intestine within days of infection, before any such changes in peripheral lymphoid tissues. The loss of CD4$^+$ T cells in the intestine occurred coincident with productive infection of large numbers of mononuclear cells at this site. The intestine appears to be a major target for SIV replication and the major site of CD4$^+$ T cell loss in early SIV infection.

It is now thought that ongoing HIV replication results in a continual loss of CD4$^+$ T lymphocytes that is nearly balanced by the production of new CD4$^+$ T lymphocytes (*1*). This model explains some of the puzzles of HIV infection, but the events that occur in the initial stage of infection remain largely unexplored. Although it is clear that HIV targets lymphoid tissue, nearly all studies in this area have focused on peripheral blood and lymph nodes. These studies overlook the fact that the gastrointestinal tract contains most of the lymphoid tissue in the body (*2*, *3*). Furthermore, it is likely that the behavior of HIV in the unique immunologic environment of the intestinal mucosa differs from that observed in the periphery.

The gut-associated lymphoid tissue (GALT) consists of organized lymphoid tissue (Peyer's patches and solitary lymphoid follicles) as well as large numbers of activated memory T lymphocytes diffusely dis-

tributed throughout both the intestinal lamina propria and epithelium. The proportion of activated memory $CD4^+$ T cells is much greater in the intestinal lamina propria than in peripheral blood or lymph nodes (*2*, *4*–*6*). Because HIV replicates most efficiently in activated memory $CD4^+$ T cells (*7*), the intestinal tract may be the preferred target for initial infection and replication of HIV. The effects of primary HIV infection on GALT are difficult to assess in humans, largely because of the difficulties involved in examining the intestinal tract within days of infection. The SIV macaque model provides a useful tool for examining the pathogenesis of acquired immunodeficiency syndrome and the early events in infection (*8*).

Groups of macaques were inoculated intravenously with the following molecular clones of SIV (*9*): pathogenic SIVmac239 (*10*); a macrophage-competent derivative of SIVmac239, designated SIVmac239/316 (*11*); and an attenuated, *nef*-deletion derivative of SIVmac239, designated SIVmac239Δ*nef* (*12*). Two animals in each group were killed at 7, 14, 21, and 50 days after inoculation. Lymphocytes were separately harvested from the intestinal epithelium and lamina propria as well as from the blood, spleen, and both mesenteric and axillary lymph nodes of each animal (*13*). Although intestinal intraepithelial lymphocytes (IELs) and lamina propria lymphocytes (LPLs) were collected and analyzed separately, only minor changes were detected in the IEL population (*14*); thus, only the LPL data are presented here. Lymphocytes from all tissues were examined for expression of CD3 (a pan–T cell marker), CD4 (T helper cells), CD8 (cytotoxic/suppressor cells), CD25 (interleukin-2 receptor, activated T cells), and CD45RA (naïve T cells) by multiparameter flow cytometry (*13*). To localize virus and examine the numbers and phenotypes of infected cells, we performed in situ hybridization for SIV and immunohistochemistry on intestine and peripheral lymphoid tissues (*15*).

Infection with pathogenic SIV (SIVmac239 or SIVmac239/316) consistently resulted in rapid and profound depletion of $CD4^+$ cells exclusively in the lamina propria of the intestinal tract (jejunum, ileum, and colon) (Fig. 1A). These declines were evident by 7 days after infection, as compared to controls or animals infected with SIVmac239Δ*nef* ($P < 0.01$) (*16*). The nadir of intestinal CD4 depletion was reached by 14 to 21 days after infection in SIVmac239-infected animals but was delayed to 50 days in SIVmac239/316-infected animals.

Immunohistochemistry on intestinal segments confirmed the $CD4^+$ T cell depletion in the lamina propria and to a lesser extent in the Peyer's patches and solitary lymphoid nodules (*14*). Immunohistochemistry and quantitative analysis of CD3 did not reveal any significant change in the total number of T cells in the intestine (*14*). These results, in conjunction with the observed increase in the percentage of $CD8^+$ T cells (Fig. 1), indicate that the $CD4^+$ T cell depletion was accompanied by an increase in absolute numbers of $CD8^+$ T cells.

In marked contrast, there were minimal changes in the percentages of $CD4^+$ lymphocytes in the blood, spleen, and lymph nodes from these same animals at the same time points. Slight decreases in $CD4^+$ cells were observed in the axillary and mesenteric lymph nodes of animals infected with pathogenic clones of SIV, but these differences were not significant (Fig. 1). Percentages of $CD4^+$ T cells in the blood were increased at days 7 and 14 after infection, but the absolute numbers were not significantly altered at these time points.

To rule out the possibility of CD4 downmodulation or gp120-mediated CD4 masking in the intestinal CD4 depletion, we performed three-color analysis with antibodies to CD3, CD4, and CD8. No significant increase in the proportion of $CD3^+CD4^-CD8^-$ (double-negative) T cells was observed, which would have been expected if either CD4 masking or downmodulation were involved (Fig. 2). This strongly suggests that the $CD4^+$ T cells were eliminated from the intestinal tract by lytic or apoptotic mechanisms or, alternatively, by altered trafficking of mucosal lymphocytes.

To determine whether these results were unique to molecular clones of SIV-

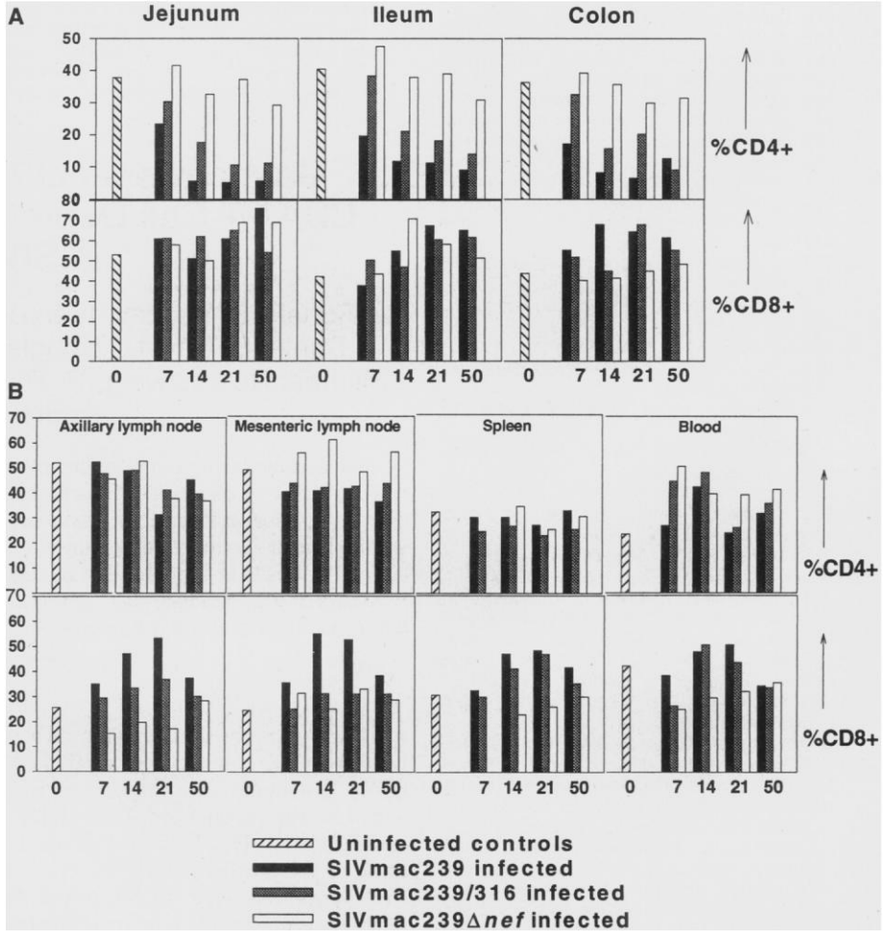

Fig. 1. Sequential changes in $CD4^+$ and $CD8^+$ T cell populations in lymphoid tissues of macaques 7, 14, 21, and 50 days after infection with molecular clones of SIV. (**A**) Intestinal lamina propria; (**B**) lymph nodes, spleen, and blood. Each bar represents the mean of two (infected) or four (uninfected control) animals.

New England Regional Primate Research Center, Harvard Medical School, 1 Pine Hill Drive, Post Office Box 9102, Southborough, MA 01772, USA.

*To whom correspondence should be addressed. E-mail: alackner@warren.med.harvard.edu

mac239, we inoculated two additional animals with uncloned SIVmac251. When these animals were killed at 14 days after infection, they also had marked $CD4^+$ T cell depletion in the intestinal lamina propria ($CD4^+$ T cell percentages decreased to 8% or less in the jejunum and colon and 15% or less in the ileum) without significant changes in peripheral lymphoid tissues (*14*). The speed and extent of the $CD4^+$ T cell depletion in these animals was indistinguishable from what was observed in animals infected with SIVmac239 (Fig. 1A). An additional three animals inoculated with SIVmac251 were killed 5 months after infection to determine whether the $CD4^+$ cells returned after the acute phase of infection. $CD4^+$ T cells were markedly decreased in the intestine of these animals as well (to less than 10% of LPLs) (*14*). Thus, intestinal $CD4^+$ T cell depletion is consistent for different pathogenic strains of SIV and appears to persist throughout the course of infection. Selective depletion of $CD4^+$ T cells from the intestine also appears to occur in HIV-infected humans. Several studies have suggested that $CD4^+$ T cell depletion is more pronounced or occurs sooner in the intestine than in peripheral blood, even in the relatively early stages (first several months) of HIV infection (*5*, *17*, *18*).

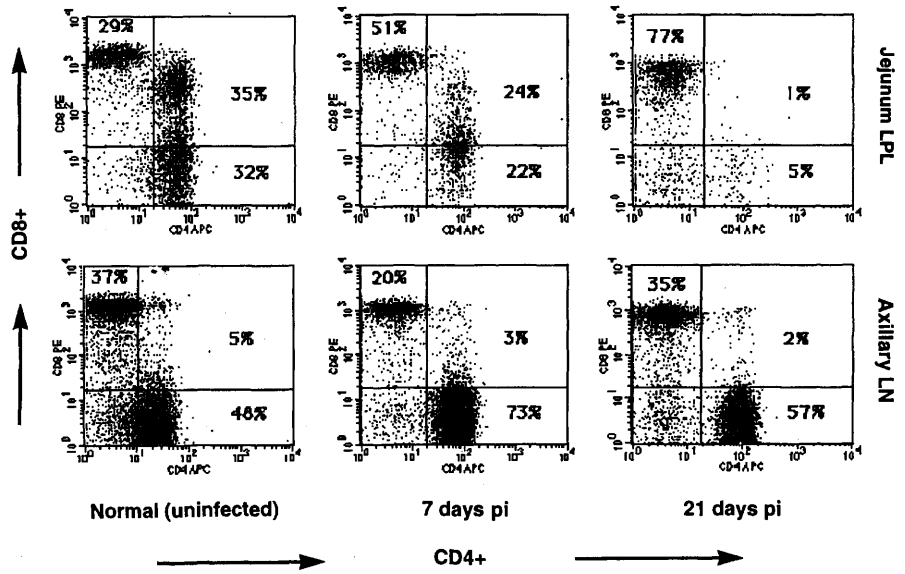

Fig. 2. Three-color flow cytometry dot plots comparing lymphocytes isolated from the intestinal lamina propria (jejunum LPL) with those from the axillary lymph node (LN) from a normal uninfected macaque and from macaques infected with SIVmac239 at 7 and 21 days after infection (pi). Each set of top and bottom panels corresponds to the same animal. Plots were generated by first gating through lymphocytes and then through $CD3^+$ T cells.

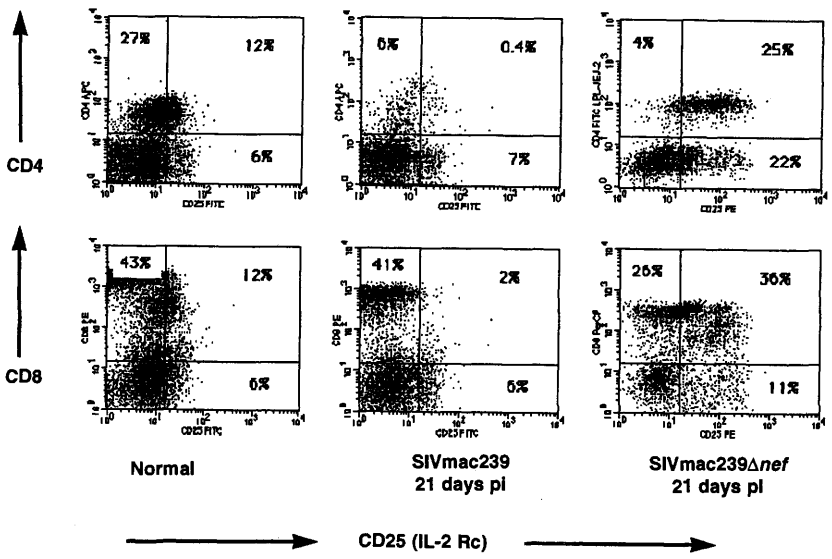

Fig. 3. Flow cytometry dot plots comparing CD25 expression on intestinal LPLs from an uninfected macaque and from macaques infected with SIVmac239 or SIVmac239Δ*nef*. Plots were generated by gating on lymphocytes.

In contrast to pathogenic SIV, infection with attenuated virus (SIVmac239Δ*nef*) did not result in a significant loss of intestinal $CD4^+$ cells (Fig. 1) but was associated with marked T cell activation, as determined by up-regulation of CD25 (interleukin-2 receptor). Marked increases in CD25 coexpression were detected in both $CD4^+$ and $CD8^+$ T cell subsets in SIVmac239Δ*nef*-infected animals (Fig. 3).

The virulence of the molecular clones used here correlated with the rapidity and degree of intestinal $CD4^+$ T cell depletion, and correlated inversely with CD25 expression on the remaining $CD4^+$ cells. Infection with SIVmac239 resulted in rapid and profound $CD4^+$ depletion in the intestine, and it decreased the relative expression of CD25 on the remaining $CD4^+$ intestinal lymphocytes. Infection with SIVmac239Δ*nef* was associated with marked up-regulation of CD25 on intestinal $CD4^+$ T cells and to a lesser extent on $CD8^+$ cells (Figs. 3 and 4). The effects of infection with SIVmac239/316 on CD25 expression were intermediate between the others, with the highest expression 21 days after infection. Infection with SIVmac239/316 resulted in more CD25 expression on $CD8^+$ cells and on the remaining $CD4^+$ T cells than did infection with SIVmac239 (Fig. 4). Expression of CD25 was consistently higher in the jejunum of both normal and SIV-infected macaques than in the ileum or colon. Furthermore, expression of CD25 was consistently higher on $CD4^+$ cells than on $CD8^+$ lymphocytes (Fig. 4). Although more organized lymphoid tissue is present in the ileum, these data suggest that jejunal lymphocytes (which are mostly LPLs) are more activated than ileal lymphocytes, which contain many organized lymphoid nodules containing fewer activated cells. This is consistent with the recent finding that CD4 depletion in the intestine of HIV-infected patients selectively occurs in the lamina propria rather than in the organized lymphoid tissue of the intestine (*18*).

Our findings also confirm that the normal intestine contains larger numbers of activated memory $CD4^+$ T cells than do peripheral lymphoid tissues. The expression of CD25 is consistently higher, and the expression of CD45RA (naïve cells) is consistently lower, on intestinal lymphocytes than on lymphocytes obtained from

the peripheral lymphoid tissues or mesenteric lymph nodes (*2*, *4*–*6*). Although a suitable memory cell marker has not been found that cross-reacts with the rhesus macaque, these data confirm that the intestinal mucosal lymphoid tissue of rhesus macaques is similar in composition to that of humans. Moreover, these data indicate that the major target cells of HIV and SIV are far more abundant in the intestinal tract than in peripheral tissues.

Further insights into the early pathogenesis of SIV were gained by examining the distribution and phenotype of SIV-infected cells in the intestine by in situ hybridization, alone and combined with immunohistochemistry, at sequential time points after SIVmac239 infection. Coinciding with the onset of CD4 depletion (7 days after infection), many SIV-infected lymphocytes were present in the intestinal tract of animals infected with pathogenic clones of SIV (Fig. 5A). Also, there were more virus-infected cells in the intestine than in the peripheral lymphoid tissues, as previously described (*19*). Initially, many infected cells were present throughout the intestinal lamina propria as well as in the T-dependent areas of organized lymphoid nodules (Peyer's patches and solitary lymphoid follicles). At later time points (21 and 50 days after infection) when $CD4^+$ T cell depletion was marked, the number of virus-infected cells was greatly diminished and the remaining infected cells were mainly limited to the organized lymphoid nodules. Conversely, the percentage of infected macrophages increased at later time points. Although infected macrophages were rare in animals at day 7 after infection, combined immunohistochemistry for macrophages (HAM-56) and in situ hybridization for SIV demonstrated an increase in the percentage of infected macrophages at later time points, which were mainly located within organized lymphoid nodules (Fig. 5B). This is consistent with the results of previous experiments using uncloned SIVmac251 (*20*).

Combined, the in situ hybridization and flow cytometry data suggest the following course of events: Initially, large numbers of activated memory $CD4^+$ T cells are constitutively present throughout the intestinal lamina propria. These initial target cells are rapidly infected and serve as sources for viral amplification and dissemination. However, this large pool of activated memory $CD4^+$ T cells in the intestine is rapidly depleted, leaving only naïve lymphocytes and macrophages to serve as viral host cells. The decrease in the pool of susceptible cells results in a decline in viral load in the tissue. However, new lymphocytes are continually recruited to or produced in the organized lymphoid tissues (GALT and lymph nodes), and these may become activated by antigenic stimulation to serve as fresh host cells for viral replication, thus perpetuating the infection. This would explain why the numbers of virus-infected lymphocytes are reduced in GALT at the later time points of infection.

These observations strongly suggest that intestinal lymphoid tissue is a crucial target organ in the initial pathogenesis of SIV infection. On the basis of this evidence, we hypothesize that the gastrointestinal tract, and not the peripheral lymphoid tissue, is the major site of early SIV and HIV replication and amplification, resulting in profound and rapid $CD4^+$ T cell loss. If so, then the acute phase of infection with SIV or HIV should be viewed primarily as a disease of the mucosal immune system. There are important ramifications of considering SIV/HIV as a mucosal disease, including the design of therapies that target the intestinal tract and vaccines that stimulate an effective mucosal immune response. These results suggest that an important advantage of a modified live virus vaccine that targets the intestinal mucosa would be its ability

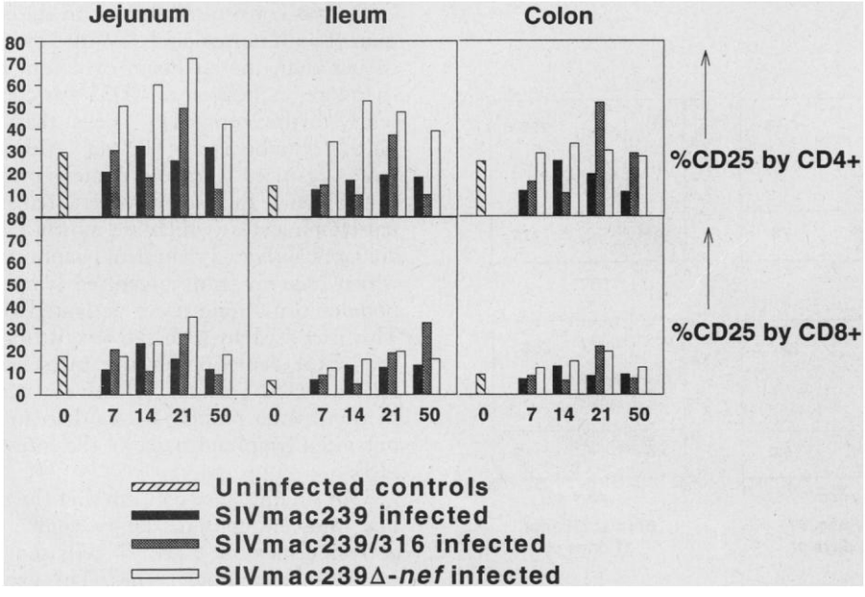

Fig. 4. CD25 expression by $CD4^+$ and $CD8^+$ lymphocytes in the intestinal lamina propria of macaques 7, 14, 21, and 50 days after infection, as measured by flow cytometry. Data were generated by first gating on $CD4^+$ or $CD8^+$ lymphocytes. Each bar represents the mean of two (infected) or four (control) animals.

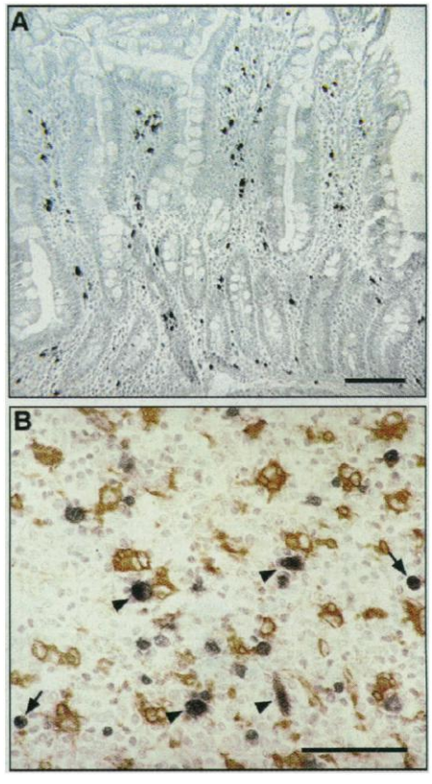

Fig. 5. Localization of SIV-infected cells in the intestine of macaques. (**A**) In situ hybridization for SIV in the jejunum showing large numbers of infected lymphocytes (black) in the lamina propria 7 days after infection with SIVmac239. Scale bar, 100 μm. (**B**) Intestinal lymphoid nodule double-labeled by in situ hybridization for SIV (black) and immunohistochemistry (brown) for HAM-56 (macrophages) in a macaque 21 days after infection with SIVmac239. Note the presence of several SIV-infected macrophages having large black nuclei and brown cytoplasm (arrowheads). A few SIV-infected lymphocytes are also visible in this field (arrows). Scale bar, 50 μm.

to stimulate an appropriate immune response at the site involved in the earliest stages of viral infection.

REFERENCES AND NOTES

1. D. D. Ho *et al.*, *Nature* **373**, 123 (1995); X. Wei *et al.*, *ibid.*, p. 117; A. Amadori, R. Zamarchi, L. Chieco-Bianchi, *Immunol. Today* **17**, 414 (1996).
2. T. T. MacDonald and J. Spencer, in *Gastrointestinal and Hepatic Immunology*, R. H. Heatley, Ed. (Cambridge Univ. Press, Cambridge, 1994), pp. 1–23.
3. N. Cerf-Bensussan and D. Guy-Grand, *Gastroenterol. Clin. N. Am.* **20**, 549 (1991); J.-P. Kraehenbuhl and M. R. Neutra, *Physiol. Rev.* **72**, 853 (1992).
4. M. Zeitz, W. C. Greene, N. J. Peffer, S. P. James, *Gastroenterology* **94**, 647 (1988); H. L. Schieferdecker, R. Ullrich, H. Hirseland, M. Zeitz, *J. Immunol.* **149**, 2816 (1992).
5. T. Schneider *et al.*, *Clin. Exp. Immunol.* **94**, 430 (1994).
6. R. S. Veazey *et al.*, *Clin. Immunol. Immunopathol.* **82**, 230 (1997).
7. J. S. McDougal *et al.*, *J. Immunol.* **135**, 3151 (1985); G. Nabel and D. Baltimore, *Nature* **326**, 711 (1987); C. J. Van Noesel *et al.*, *J. Clin. Invest.* **86** (1990); S. M. Schnittman *et al.*, *Proc. Natl. Acad. Sci. U.S.A.* **87**, 6058 (1990); Z. F. Rosenberg and A. S. Fauci, *FASEB J.* **5**, 2382 (1991).
8. R. C. Desrosiers and D. J. Ringler, *Intervirology* **30**, 301 (1989); R. C. Desrosiers, *Annu. Rev. Immunol.* **8**, 557 (1990); K. A. Reimann *et al.*, *J. Virol.* **68**, 2362 (1994); A. A. Lackner, *Curr. Top. Microbiol. Immunol.* **188**, 35 (1994).
9. In separate experiments, groups (n = 8) of juvenile (age 1 to 1.5 years) male rhesus macaques were intravenously inoculated with equal doses (50 ng of p27) of molecularly cloned SIVmac239, SIVmac239/316 (a weakly pathogenic, macrophage-competent molecular clone derived from SIVmac239), or SIVmac239Δ*nef* (an attenuated virus derived from SIVmac239 by deleting a large portion of the *nef* gene). Four age- and sex-matched, uninfected macaques were used as controls. All animals were maintained in accordance with the standards of the American Association for Accreditation of Laboratory Animal Care and the guidelines of the Committee on Animals of Harvard Medical School.
10. H. Kestler *et al.*, *Science* **248**, 1109 (1990).
11. K. Mori, D. J. Ringler, T. Kodama, R. C. Desrosiers, *J. Virol.* **66**, 2067 (1992).
12. H. W. Kestler *et al.*, *Cell* **65**, 651 (1991).
13. Lymphocytes were isolated from the intestinal epithelium, lamina propria, spleen, lymph nodes, and blood and stained for flow cytometric analysis as described (*6*). Samples were stained with monoclonal antibodies (mAbs) to human CD4 (Ortho Diagnostics), CD8, CD25, CD45RA (Becton Dickinson), and rhesus CD3 [T. Kawai *et al.*, *Transplant. Proc.* **26**, 1845 (1994)] directly conjugated to fluorescein isothiocyanate, phycoerythrin, peridinin chlorophyll protein, or allophycocyanin. Samples were analyzed using either a FACScan or Vantage flow cytometer and Cell Quest software (Becton Dickinson).
14. R. S. Veazey *et al.*, data not shown.
15. In situ hybridization for SIV and immunohistochemistry for macrophages (HAM-56, Dako), CD3, and CD4 were performed on intestinal tissues, peripheral lymph nodes, and spleen as described [C. J. Horvath *et al.*, *J. Leukocyte Biol.* **53**, 532 (1993); P. Ilyinskii *et al.*, *J. Virol.* **68**, 5933 (1994); J. H. Lane *et al.*, *Am. J. Pathol.* **149**, 1097 (1996)]. Absolute numbers of $CD3^+$ T cells were quantitated per square micrometer of intestinal lamina propria by computer-assisted image analysis, as described (*6*). Only LPLs were quantitated because of the technical difficulties involved in discriminating positive cells in Peyer's patches and lymphoid follicles.
16. Statistical analyses were accomplished by means of a Kruskal-Wallis one-way analysis of variance using commercial computer software (Sigma Plot, Jandel). Analyses were performed by comparing the percentages of $CD4^+$ cells of all lamina propria samples (three per animal; jejunum, ileum, and colon) from uninfected normal (n = 12), SIVmac239-infected (n = 6), and SIVmac239Δ*nef*-infected (n = 6) macaques.
17. S. G. Lim *et al.*, *Clin. Exp. Immunol.* **92**, 448 (1993); M. Schrappe-Bacher *et al.*, *J. Acquired Immune Defic. Syndr. Hum. Retrovirol.* **3**, 238 (1990); T. Schneider *et al.*, *Gut* **37**, 524 (1995); V. D. Rodgers, R. Fassett, M. F. Kagnoff, *Gastroenterology* **90**, 552 (1986); F. Clayton *et al.*, *ibid.* **103**, 919 (1992).
18. F. Clayton, G. Snow, S. Reka, D. P. Kotler, *Clin. Exp. Immunol.* **107**, 288 (1997).
19. V. G. Sasseville *et al.*, *Am. J. Pathol.* **149**, 163 (1996).
20. C. Heise, P. Vogel, C. J. Miller, C. H. Halsted, S. Dandekar, *ibid.* **142**, 1759 (1993).

21. We thank K. Toohey and A. Hampson for photographic assistance, J. Wong for rhesus CD3 mAb, and P. Sehgal and the animal care staff at the New England Regional Primate Research Center for their excellent care of the animals. Supported by NIH grants DK50550, AI38559, AI25328, RR07000, and RR00168. A.A.L. is the recipient of an Elizabeth Glaser Scientist Award.

7 November 1997; accepted 20 February 1998

Association of the AP-3 Adaptor Complex with Clathrin

Esteban C. Dell'Angelica, Judith Klumperman, Willem Stoorvogel, Juan S. Bonifacino*

A heterotetrameric complex termed AP-3 is involved in signal-mediated protein sorting to endosomal-lysosomal organelles. AP-3 has been proposed to be a component of a nonclathrin coat. In vitro binding assays showed that mammalian AP-3 did associate with clathrin by interaction of the appendage domain of its β3 subunit with the amino-terminal domain of the clathrin heavy chain. The β3 appendage domain contained a conserved consensus motif for clathrin binding. AP-3 colocalized with clathrin in cells as observed by immunofluorescence and immunoelectron microscopy. Thus, AP-3 function in protein sorting may depend on clathrin.

The formation of vesicles for transport between organelles of the endocytic and secretory pathways and the selection of cargo for packaging into those vesicles are mediated by protein coats associated with the cytosolic face of the organelles (*1*). The best characterized coats contain clathrin and protein complexes termed "adaptors" (*2*). Clathrin is a complex of three heavy chains and three light chains that polymerizes to form the scaffold of the coats. The adaptors mediate attachment of clathrin to membranes and recruit integral membrane proteins to the coats. Two clathrin adaptors have been described to date—AP-1 and AP-2, which participate in protein transport to the endosomal-lysosomal system from the trans-Golgi network (TGN) and the plasma membrane, respectively.

Recently, another complex related to AP-1 and AP-2 has been identified. This complex, termed AP-3, is composed of two large subunits (δ and β3A or β3B), a medium-sized subunit (μ3A or μ3B), and a small subunit (σ3A or σ3B) (*3–8*). AP-3 has been localized to the TGN and endosomes (*4, 5*) and is involved in protein trafficking to lysosomes or specialized endosomal-lysosomal organelles such as pigment granules, melanosomes, and platelet dense granules (*8, 9*). Previous studies suggested that AP-3 is a component of a nonclathrin coat (*3, 4*). However, a critical question has remained unanswered: does AP-3 assemble with a structural coat protein that plays the role of clathrin?

We used glutathione S-transferase (GST) fusion proteins bearing the H (hinge) and C (COOH-terminal) segments of the "appendage" region of human β3A (*6*) to search for this putative protein (Fig. 1A). The reason for selection of these constructs was that both AP-1 and AP-2 bind clathrin via the appendage regions of the β1 and β2 subunits (*10, 11*). Affinity purification from a cytosolic extract of a human T cell line, Jurkat, resulted in isolation of a prominent 180-kD protein on GST-$\beta3A_C$ but not GST-$\beta3A_H$ or GST columns (Fig. 1B). Unexpectedly, microsequencing of eight tryptic peptides derived from the 180-kD protein identified it as the clathrin heavy chain (Fig. 1B) (*12*). Binding of clathrin to GST-$\beta3A_C$ could also be demonstrated by immunoblotting with antibodies to either the heavy (Fig. 1C, IB, and Fig. 1D, TL..) or light (Fig. 1D, CON.1) chain of clathrin as well as by immunoprecipitation of metabolically labeled proteins (Fig. 1C, IP). Furthermore, the extent of clathrin binding to GST-$\beta3A_C$ was comparable to that of a GST fusion protein having the

E. C. Dell'Angelica and J. S. Bonifacino, Cell Biology and Metabolism Branch, National Institute of Child Health and Human Development, National Institutes of Health, Bethesda, MD 20892, USA.
J. Klumperman and W. Stoorvogel, Department of Cell Biology, School of Medicine, Institute of Biomembranes, Utrecht University, 3584 CX Utrecht, The Netherlands.
*To whom correspondence should be addressed. E-mail: juan@helix.nih.gov